Available online at www.sciencedirect.com
ScienceDirect
Journal of Applied Geophysics 66 (2008) 188–196
JOURNAL OF APPLIED GEOPHYSICS
www.elsevier.com/locate/jappgeo

A laboratory study of the effect of magnetite on NMR relaxation rates

Kristina Keating *, Rosemary Knight

Department of Geophysics, Stanford University, Mitchell Building, Stanford, CA, 94305, United States

Received 6 February 2007; accepted 8 September 2007

Abstract

We conducted a laboratory study to measure the effect of magnetite concentration and grain size on proton nuclear magnetic resonance (NMR) relaxation rates of sand mixtures and to determine the dominant mechanism by which relaxation occurs. We measured mixtures of quartz and three different forms of magnetite: a powdered synthetic magnetite; a small-grained, natural magnetite; and a large-grained, natural magnetite. The powdered synthetic magnetite was mixed with quartz in five concentrations ranging from 0.14 to 1.4% magnetite by weight; both sizes of natural magnetite were mixed with quartz in concentrations of 1 and 2% magnetite by weight. The NMR response of the water-saturated samples was measured and used to calculate four averaged relaxation rates for each magnetite concentration: the total mean log, bulk fluid, surface, and diffusion relaxation rates. The results of this study show that: 1) surface relaxation was the dominant relaxation mechanism for all samples except the powdered synthetic magnetite sample containing 1.4% magnetite; 2) the surface relaxivity is a function of the fraction of the surface area in the sample composed of magnetite; 3) there is no clear dependence of the diffusion relaxation rate on the concentration of magnetite.

Keywords: NMR; Magnetite; Transverse relaxation; Grain size

1. Introduction

Proton nuclear magnetic resonance (NMR) is a technique that can be used to detect the presence of hydrogen nuclei and to obtain information about their physiochemical environments. In a water-saturated geologic material the NMR relaxation measurement involves monitoring the relaxation, or return to equilibrium, of the bulk nuclear magnetization of the hydrogen nuclei in the pore water after the sample has been perturbed with a radio-frequency pulse. NMR relaxation measurements can be made in the laboratory or in the field using a well-logging device or a system deployed at Earth's surface. The well-logging system has been used for a number of years in the petroleum industry to determine reservoir permeability (e.g. Seevers, 1966; Timur, 1969; Korb et al., 2003) and has recently been used for hydrogeophysical applications (Clayton, 2006). The surface-based system, referred to as MRS (magnetic resonance sounding), has been used to estimate hydraulic conductivity in the top ~ 100m of Earth (e.g. Shushakov, 1996; Legchenko et al., 2002).

Of interest in our research is the effect of magnetite (Fe_3O_4), a commonly occurring oxide, on the NMR relaxation measurement for geological materials. It is well known that the NMR relaxation rate of a material can be affected by the presence of paramagnetic ions such as Fe(III), and by contrasts in magnetic susceptibility between the pore water and the solid phase. Magnetite contains Fe (III) and has a large magnetic susceptibility, so it is not surprising that, in a study by Keating and Knight (2007), the addition of magnetite to quartz sand was found to have a significant effect on the relaxation rate. This previous study compared the relaxation behavior of five iron-oxide minerals including magnetite and found that the presence of magnetite had a much stronger effect on the relaxation rate than the presence of the other iron-oxides. The objective of this study was to extend the previous by determining the specific mechanism/s by which magnetite impacts the NMR relaxation rate.

We conducted laboratory experiments using quartz sand mixed with known concentrations of magnetite. We limited our measurements to magnetite concentrations of less than 2%

* Corresponding author. Tel.: +1 650 724 9939; fax: +1 650 725 7344.
E-mail addresses: kkeat@stanford.edu (K. Keating), rknight@stanford.edu (R. Knight).

0926-9851/$ - see front matter © 2007 Elsevier B.V. All rights reserved.
doi:10.1016/j.jappgeo.2007.09.001

which is representative of the magnetite concentrations found in natural environments (Thompson and Oldfield, 1986). Because magnetite can be present in soils as small crystals formed by biogeochemical processes (Oldfield, 1999; Evans and Heller, 2003) or as large grains from anthropogenic sources or physical weathering, we tested three grain sizes by using a powdered synthetic magnetite, a small-grained natural magnetite and a large-grained natural magnetite. These measurements advanced our understanding of the effect of magnetite on NMR relaxation data; knowledge that is essential if we are to obtain accurate information from NMR data in many geologic environments.

2. Background and theory

2.1. NMR relaxation theory

Proton NMR detects the presence of hydrogen nuclei; for hydrogeophysical applications the ability to detect hydrogen nuclei is of interest due to the presence of hydrogen in water. Each hydrogen nucleus, composed of a single proton, possesses a nuclear spin angular momentum. When in a static magnetic field, B_0, the nuclear spins in water precess about the static field. The nuclear spins precess at the Larmor frequency, f_0, which is related to B_0 by

$$f_0 = \gamma |B_0| / (2\pi) \tag{1}$$

where γ is the gyromagnetic ratio for hydrogen protons in water molecules (γ = 0.267rad/[nT·s]). For MRS instruments f_0 ranges from 0.8 to 2.8kHz; for NMR well-logging instruments f_0 ranges from 0.5 to 2MHz; for most laboratory instruments f_0 ranges from 0.01 to 900MHz. If a weak magnetic field oscillating at f_0 is applied the nuclear spins will tilt away from their equilibrium position. Once the oscillating field is removed the nuclear spins will return, or relax, to their equilibrium position. The return to equilibrium results in a measurable signal from the bulk nuclear magnetization, which can be described in terms of the transverse magnetization, M_{xy}.

For a bulk fluid the return to equilibrium behaves as an exponential decay:

$$M_{xy}(t) = M_0 \exp(-t/T_{2B}) \tag{2}$$

where M_0 is the initial magnetization, t is time and T_{2B} is the bulk fluid relaxation time; the inverse, T_{2B}^{-1}, is referred to as the bulk fluid relaxation rate. M_0 is proportional to the total number of hydrogen nuclei in the bulk water. The magnitude of T_{2B}^{-1} for a fluid is controlled by dipole–dipole molecular interactions and depends on the viscosity of the fluid, the concentration of dissolved paramagnetic species (such as dissolved oxygen, Mn (II) ions or Fe(III) ions) and pH (Bloembergen et al., 1948).

For water confined in a pore, the measured relaxation rate is generally found to be greater than the bulk fluid relaxation rate due to two mechanisms that can enhance relaxation: surface relaxation and diffusion relaxation. In a single pore, the relaxation rate of water, T_2^{-1}, is described as a sum of relaxation rates (Brownstein and Tarr, 1979):

$$T_2^{-1} = T_{2B}^{-1} + T_{2S}^{-1} + T_{2D}^{-1} \tag{3}$$

where T_{2S}^{-1} represents the surface relaxation rate and T_{2D}^{-1} represents the diffusion relaxation rate. Eq. (3) is valid for samples in the fast diffusion regime, which assumes that all protons travel to and interact with the solid surface within the time interval of the NMR experiment. For water in a porous geological material with a range of pore sizes, a multiexponential decay is observed,

$$M_{xy}(t) = \sum_i m_i \exp(-t/T_{2i}). \tag{4}$$

Here m_i is proportional to the number of moles of hydrogen relaxing with rate T_{2i}^{-1}. The total number of moles of hydrogen is proportional to $M_{xy}(0) = \Sigma m_i$. The values of m_i versus T_{2i} are often plotted to show the distribution of relaxation times. In studies of the NMR response of porous materials, the arithmetic mean of log T_{2i}, T_{2ML}, is typically calculated from the distribution of relaxation times and used to represent the relaxation behavior. Eq. (3) then becomes:

$$T_{2ML}^{-1} = T_{2B}^{-1} + T_{2S}^{-1} + T_{2D}^{-1} \tag{5}$$

where rates are now taken to be average values for the entire pore space of the sample material instead of a single pore. While the magnitude of T_{2B}^{-1} is determined by the properties of the pore fluid, the magnitudes of T_{2S}^{-1} and T_{2D}^{-1} are strongly affected by the properties of the solid phase and controlled by very different relaxation mechanisms, referred to as the surface and diffusion relaxation mechanisms. Central to our research is the question of how the presence of magnetite influences these mechanisms. In the next sections we briefly review the way in which the properties of a geological material determine surface and diffusion relaxation rates.

2.2. Surface relaxation

The surface relaxation rate is determined by interactions that occur between the hydrogen nuclei in water and the solid surface of the geologic material. In the case of fast diffusion the surface relaxation rate is given by (Senturia and Robinson, 1970; Brownstein and Tarr, 1979),

$$T_{2S}^{-1} = \rho_2 S/V \tag{6}$$

where S/V is the surface-area-to-volume ratio of the water-filled pore-space and ρ_2 is the surface relaxivity. For the fast diffusion assumption to be valid, the following relationship must be satisfied: $\rho_2 V/S \ll D$, where D is the self-diffusion coefficient of water ($D = 2.5 \times 10^{-5}$ for water at 30°C). The relationship between the surface relaxation time and the surface-area-to-volume ratio shown in Eq. (6) is the basis for the use of NMR relaxation times to estimate permeability (e.g. Seevers, 1966; Timur, 1969) and hydraulic conductivity (e.g. Legchenko et al., 2002).

Current NMR theory associates ρ_2 with the presence of paramagnetic species (i.e. unpaired electrons) on the surfaces of the pore-space (Brownstein and Tarr, 1979; Godefroy et al., 2001). Laboratory studies of samples with known concentrations of paramagnetic ions, both in solid grains and adsorbed to

the surface of solid grains, have shown that the surface relaxivity is proportional to the surface concentration of paramagnetic ions (Foley et al., 1996). Due to the presence of the paramagnetic species Fe(III) in magnetite we would expect ρ_2, and thus T_{2S}^{-1}, of a sample to change as the concentration of magnetite in the sample changes.

2.3. Diffusion Relaxation

The diffusion relaxation rate is determined by the effect of the magnetic properties of the solid phase on the diffusing water molecules and is related to the average internal gradient of the magnetic field, G, by,

$$T_{2D}^{-1} = D(\gamma G t_E)^2/12 \quad (7)$$

where t_E is the echo-time, a rephasing parameter used during the Carr–Purcell–Meiboom–Gill (CPMG) pulse sequence (Carr and Purcell, 1954; Meiboom and Gill, 1958). (This pulse sequence was developed to rephase proton spins in a solid in the presence of non-uniform magnetic fields). Internal gradients are caused by a magnetic susceptibility contrast between the pore water and the solid phase. Because of the large magnetic susceptibility of magnetite even a small concentration of magnetite could result in the presence of internal gradients.

The presence of magnetic domains in magnetite causes the magnetic susceptibility to be grain size dependent. The magnetic domains are classified as superparamagnetic, single domain and multidomain. Although it is difficult to define the exact grain size separating the different domain states, in general, nano-size particles are superparamagnetic, single crystals with diameters ranging from 0.07 to 0.7μm are single domain, and massive grains with diameters greater than 10μm are multidomain (Hunt et al., 1995; Smith, 1999). Using these definitions the powdered synthetic magnetite samples used in this study were single domain grains; both grain sizes of the natural magnetite samples used in this study were multidomain grains.

3. Methods and materials

The objective of this study was to determine the relaxation mechanism/s responsible for the large effect of magnetite on the NMR relaxation rate of a geological material. That is, is the dramatically enhanced relaxation rate in the presence of magnetite due primarily to surface relaxation, diffusion relaxation, or both. To assess the contributions from the two relaxation mechanisms we conducted a laboratory experiment and compared the magnitude of the averaged relaxation rates, T_{2ML}^{-1}, T_{2B}^{-1}, T_{2S}^{-1},and T_{2D}^{-1} for water saturated samples containing known concentrations of magnetite. In addition to the NMR measurements, we also measured the surface area and magnetic susceptibility of the samples, two key parameters affecting T_{2S}^{-1} and T_{2D}^{-1}.

3.1. Preparation of magnetite and quartz mixtures

The laboratory samples used in this study were prepared from mixtures of quartz sand and magnetite. Quartz sand (99.995% SiO_2, > 40 mesh, silicon (IV) dioxide, Alfa Aesar) was used as an analog for a naturally occurring mineral surface. This quartz sand has previously been used for measurements in our laboratory and we have fully characterized its NMR response (Bryar and Knight, 2003; Keating and Knight, 2007). The quartz sand was rinsed with a weak acid solution (10% HCl and deionized water) to remove paramagnetic species then mixed with magnetite. A measurement on this quartz sand from the previous study by Keating and Knight (2007) was used in this study.

One type of magnetite used in this study was powdered synthetic magnetite, obtained from Fisher Scientific. The powdered synthetic magnetite was mixed with quartz sand to obtain samples containing 0.14, 0.42, 0.71, 0.97 and 1.4% magnetite by weight.

The other type of magnetite used in this study was in the form of grains derived from natural magnetite; these grains were prepared by Christina Trotter for use in a Master's thesis (Trotter, 2001). Two types of mixtures were prepared using the natural magnetite: small-grained natural magnetite and large-grained natural magnetite. The natural magnetite was initially in the form of large pieces of magnetite obtained from Pacific Mineral Museum (Vancouver, Canada). This magnetite was from a deposit in Texada, Gilles Bay, British Columbia, Canada. The magnetite was broken into cubic centimeter-sized pieces using a rock hammer then reduced in size using a stainless steel rock grinder. The magnetite was sieved for 30min in copper sieves to isolate grain diameters of 110μm to 360μm. A portion of these grains were used to create the large-grained natural magnetite mixtures. The remaining magnetite grains were further reduced in size using an alumina ceramic rock grinder. The magnetite was then sieved to isolate grain diameters of less than 45μm; these grains were used to create the small-grained natural magnetite mixtures. Both sizes of natural magnetite grains were mixed with quartz sand to create samples containing 1 and 2% magnetite by weight. It was difficult to create samples with precisely 1 and 2% magnetite for the large-grained natural magnetite due to the large grain size and small concentration of this magnetite; the error on the magnetite concentration of these samples is higher than the error on the magnetite concentration of the samples containing small-grained natural magnetite and powdered synthetic magnetite.

3.2. NMR measurement procedures

Two NMR samples were prepared from each magnetite mixture by packing a weighed amount of the mixture into cylindrical Teflon sample holders of interior diameter 2.1cm and height 6cm. The mass of each NMR sample ranged from 28.82 to 30.93g. Each sample was saturated with deionized water. The saturation process involved submerging the sample (in the sample holder) in a beaker of deionized water, placing the beaker in a vacuum chamber and reducing the pressure in the chamber to 75mmHg for 30min. This saturation process was repeated twice. NMR measurements were made one hour following saturation.

NMR relaxation data were collected using a 2.2MHz Maran Ultra NMR Core Analyzer (Resonance Instruments) using a CPMG pulse sequence. The CPMG pulse sequence consists of applying a 90° pulse followed by a series of 180° pulses separated by t_E. A single data point was obtained at each echo in the CPMG pulse sequence; 32,000 echoes were used. Data were collected at six echo-times, t_E = 300, 400, 500, 600, 700 and 800μs, resulting in pulse sequence durations ranging from 9.6 to 25.6s. The data were stacked 100 times to improve the signal to noise ratio. A 10s delay time between each pulse sequence was used to ensure that the sample had returned to thermal equilibrium prior to the start of the next pulse sequence. All NMR measurements were made at 30°C.

Once the NMR measurements had been completed on the saturated samples the pore water was removed from each sample by centrifuging and the extracted water was used to measure T_{2B}^{-1}. Data were collected at four echo times, t_E = 300, 400, 600, and 800μs. The NMR samples were then dried overnight.

4. Sample characterization and material analysis

4.1. Porosity and surface area

The measured porosity for each sample is given in Table 1. The porosity for each sample was calculated by

$$\phi = V_p/V_s \tag{8}$$

where V_p is the volume of the pore space and V_s is the known volume of the sample holder. V_p was obtained from gravimetric measurements of the sample prior to and following saturation. The porosities ranged from 0.45 to 0.52 for both the synthetic and natural magnetite mixtures.

One subsample, approximately 33% by weight of the total sample, was taken from each NMR sample for surface area analysis. Surface area measurements were also made on two samples of both the synthetic and natural magnetite. The specific surface area, S_s, defined as the surface area normalized by the mass of the sample, was measured using a Micromeritics ASAP 2020 Accelerated Surface Area and Porosimetry System which produces accurate results for samples with a total surface area as low as 1m^2. All samples were measured using the Brunauer–Emmett–Teller (BET) adsorption method with N_2(g) as the adsorbate.

The specific surface areas of the magnetite and quartz mixtures and the pure quartz sample are given in Table 1. The specific surface area of the pure quartz sample is 0.15m^2/g. The samples containing powdered synthetic magnetite have specific surface areas ranging from 0.18 to 0.25m^2/g where increases in S_s roughly correspond to increases in magnetite concentration. The specific surface areas of the samples containing small-grained natural magnetite are 0.15m^2/g for the sample containing 1% magnetite and 0.18m^2/g for the sample containing 2% magnetite. The specific surface areas of the samples containing large-grained natural magnetite are 0.18m^2/g for the sample containing 1% magnetite and 0.19m^2/g for the sample containing 2% magnetite.

The S_s measurements on the pure magnetite samples revealed that the S_s values of the powdered synthetic magnetite were larger than the S_s values of both sizes of the natural magnetite. The specific surface area of the synthetic magnetite was 6.6m^2/g, the specific surface area of the small-grained natural magnetite was 1.1m^2/g, and the specific surface area of the large-grained natural magnetite was 0.12m^2/g.

The measured specific surface area was used to calculate S/V, also in Table 1, from

$$S/V = m_s S_s/V_p \tag{9}$$

where m_s is the total mass of the solid component.

4.2. Magnetic susceptibility measurements

Three subsamples of each mixture were taken for magnetic susceptibility measurements: one subsample from each NMR sample and one sample from the remaining mixture. Each sample was packed into a box with a volume of 6cm^3. The mass specific magnetic susceptibility, χ_m, was measured using a Sapphire SI-2 Susceptibility Instrument at the United States Geological Survey in Menlo Park, CA. This instrument produces a peak field of 1.0×10^{-4}T at a frequency of 800Hz and measures susceptibilities ranging from 10^{-6} to 1 in cgs units. Three measurements made on each sample were averaged to find χ_m; prior to each measurement the baseline magnetic field was measured. An empty container was also measured to obtain a calibration factor which was used to correct for the geometry of the sample holder.

The measurements of mass specific magnetic susceptibility versus the magnetite concentration are shown in Fig. 1. The susceptibility meter returned χ_m in units of cgs per gram; the output χ_m was multiplied by $4\pi \times 10^{-3}$ to obtain χ_m in m^3/kg. For all the magnetite mixtures, χ_m increases with increasing magnetite concentration and is in the range of 0.70×10^{-6} to 15.0×10^{-6} m^3/kg. For the powdered synthetic magnetite mixtures there is a distinct linear relationship between χ_m and magnetite concentration; this is predicted from mixture theories (Berryman, 1995; Crook et al., 2002). The error in the magnetic susceptibility measurements is below the size of the data point.

Table 1
Specific surface area (S_s), porosity (ϕ), and surface-area-to-volume ratio (S/V) for the quartz and magnetite mixtures

	Quartz	Powdered, synthetic magnetite					Small-grained magnetite		Large-grained magnetite	
Weight % magnetite	0	0.14	0.42	0.71	0.97	1.4	1	2	1	2
S_s (m^2/g)	0.15±0.02 [a]	0.18±0.02	0.18±0.02	0.20±0.02	0.24±0.02	0.25±0.01	0.15±0.01	0.18±0.01	0.18±0.02	0.19±0.01
ϕ	0.48±0.02 [a]	0.45±0.02	0.46±0.01	0.52±0.02	0.46±0.01	0.46±0.03	0.45±0.01	0.46±0.01	0.48±0.02	0.48±0.01
S/V (μm^{-1})	0.48±0.06 [a]	0.58±0.04	0.56±0.03	0.54±0.02	0.75±0.02	0.79±0.02	0.46±0.01	`0.56±0.02	0.53±0.02	0.57±0.02

[a] Data previously reported in Keating and Knight (2007).

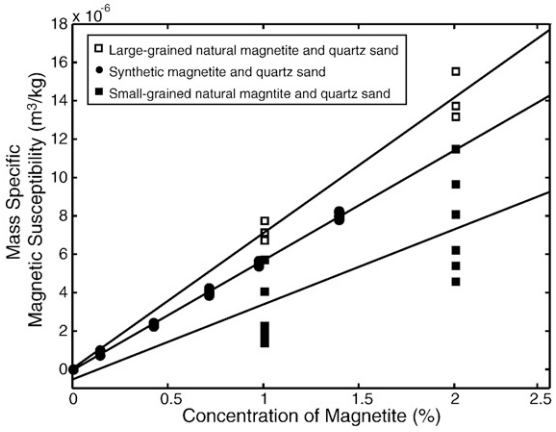

Fig. 1. Magnetic susceptibility versus the concentration of magnetite for the magnetite and quartz mixtures. The errorbars are within the size of the data point.

However, there is a large variability in χ_m for the small-grained natural samples consequently, χ_m for three additional samples of each concentration were measured. The large variability in these samples is attributed to the tendency of the small-grained natural magnetite particles to aggregate; this results in high levels of inaccuracy in the reported magnetite concentration. There is also variability in χ_m for the large-grained natural samples; this variability is due to the difficulty in preparing samples with precisely 1 and 2% magnetite for the large-grain natural magnetite due to the large grain size and small concentration of this magnetite. The differences between χ_m for the powdered synthetic magnetite and both sizes of the natural magnetite are likely due to differences in grain size, crystal shape, and impurities in the natural magnetite (e.g. titanium or aluminum substitution) (Dearing, 1999).

5. NMR results

Each NMR dataset from the water-saturated samples was fit to a distribution of 200 exponentially spaced T_2 values ranging from 1ms to 10s using the regularized non-negative least-squares inversion routine developed by Whittall et al. (1991). This approach does not enforce a specific number of relaxation times but instead allows any number of relaxation times between 0 and 200. The relaxation time distributions measured at $t_E = 300\mu s$ for all sample types as well as the relaxation time distribution for quartz sand measured in Keating and Knight (2007) are shown in Fig. 2. The relaxation time distributions for all the magnetite and quartz mixtures are broader than the relaxation time distribution for quartz sand. For both the powdered synthetic magnetite mixtures and the small-grained natural magnetite mixtures, the relaxation time distributions are broad, indicating that they consist of multiple super-imposed peaks. The relaxation time distributions for the large-grained natural magnetite mixtures are much narrower and have two super-imposed peaks separated by approximately one decade. The T_{2ML}^{-1} values for the samples were determined from the relaxation time distributions; we use these values to assess trends in the behavior of each sample.

The NMR datasets from the extracted fluids were fit using the regularized non-negative least-squares algorithm. The relaxation time distributions were found to either consist of a single relaxation time or to be narrow peaks. The T_{2B}^{-1} values, determined from the mean log average of the distributions, showed no dependence on echo time.

The T_{2ML}^{-1} and T_{2B}^{-1} values for the samples were used to calculate the T_{2S}^{-1} and T_{2D}^{-1} values. The magnitude of the T_{2S}^{-1} and T_{2D}^{-1} values were calculated by measuring the dependence of T_{2ML}^{-1} on echo time t_E for each sample. As can be seen from Eqs. (5) and (7), a plot of T_{2ML}^{-1} versus the square of the echo-time, t_E^2, will yield a straight line with a slope equal to $D(\gamma G)^2/12$ and an intercept equal to $T_{2S}^{-1} + T_{2B}^{-1}$. The T_{2ML}^{-1} values for all the mixtures show a significant dependence on t_E^2. This indicates that the presence of magnetite causes internal gradients in the magnetic field ($G \neq 0$), as expected given its high magnetic susceptibility. The intercept obtained ($T_{2S}^{-1} + T_{2B}^{-1}$) from the least squares fit of T_{2ML}^{-1} versus t_E^2 was used to calculate T_{2S}^{-1}. The slope, $D(\gamma G)^2/12$, of T_{2ML}^{-1} versus t_E^2, was used in Eq. (5) to calculate T_{2D}^{-1} at $t_E = 300\mu s$.

The relaxation rates, T_{2ML}^{-1}, T_{2B}^{-1}, T_{2S}^{-1}, and T_{2D}^{-1}, are shown versus the magnetite concentration in Fig. 3 for the powdered synthetic magnetite mixtures and in Figs. 4 and 5 for the small- and large-grained natural magnetite mixtures respectively. Both the T_{2ML}^{-1} and the T_{2D}^{-1} values shown are at $t_E = 300\mu s$. The error on each relaxation rate is the standard deviation calculated from repeated measurements; errors not shown are smaller than the data point. For all the magnetite mixtures, T_{2ML}^{-1} increases as the concentration of magnetite increases. The T_{2ML}^{-1} values also decrease with increasing grain size; the T_{2ML}^{-1} for the large-grained natural magnetite mixtures are an order of magnitude smaller than the T_{2ML}^{-1} values for the small-grained natural samples and two orders of magnitude smaller than the T_{2ML}^{-1} values for the powdered synthetic samples. In the following sections we will compare the T_{2B}^{-1}, T_{2S}^{-1}, and T_{2D}^{-1}, values for the samples to determine the dominant relaxation mechanism/s and to further explore the differences between magnetite grain sizes.

Let us first consider the ways in which the relaxation rates, T_{2B}^{-1}, T_{2S}^{-1} and T_{2D}^{-1}, of the powdered synthetic magnetite mixtures, measured at $t_E = 300\mu s$ (shown in Fig. 3), vary with magnetite concentration. We make the following observations: 1) T_{2B}^{-1} does not show a dependence on magnetite concentration and accounts for less than 1% of the total relaxation rate; 2) T_{2S}^{-1} shows an overall increase with increasing magnetite concentration; 3) T_{2D}^{-1} shows little change with magnetite concentration for concentrations less than 1.4% and a large increase at a concentration of 1.4%. When we consider the relative magnitude of T_{2S}^{-1} and T_{2D}^{-1}, we find that for all mixtures the T_{2S}^{-1} values are larger than both the T_{2D}^{-1} and T_{2B}^{-1} values; T_{2S}^{-1} accounts for over 85% of the total relaxation rate for the mixtures containing less than 1.4% magnetite, and accounts for 67% of the total relaxation rate for the mixture containing 1.4% magnetite. As would be expected from Eq. (7), T_{2D}^{-1} increases as the echo time increases. At the largest echo time used in our measurements, $t_E = 800\mu s$, the T_{2S}^{-1} values remain larger than both the T_{2D}^{-1} and T_{2B}^{-1} values and account for over 65% of the total relaxation rates for the mixtures containing less than 1.4% powdered synthetic

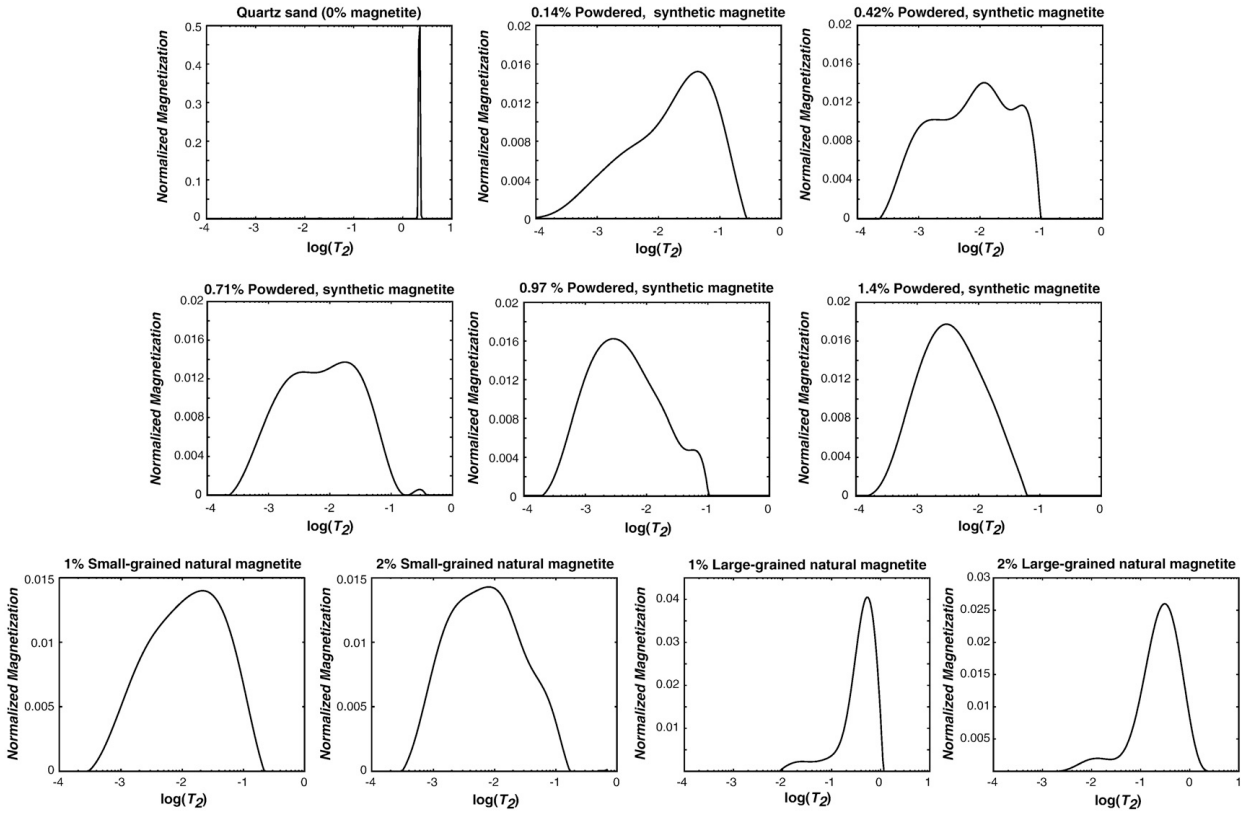

Fig. 2. Relaxation time distributions for the magnetite and quartz mixtures. The relaxation time distributions shown were measured at t_E=300 μs. The quartz mixture shown was measured in Keating and Knight (2007).

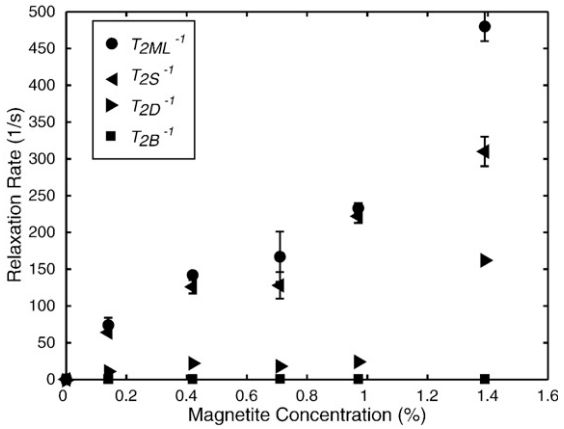

Fig. 3. Mean log average, surface, diffusion and bulk fluid relaxation rates versus magnetite concentration for water-saturated quartz mixed with powdered synthetic magnetite. Errorbars not shown are smaller than the size of the data point.

magnetite. For the mixture containing 1.4% powdered synthetic magnetite at t_E = 800μs, T_{2S}^{-1} only accounts for 22% of the total relaxation time whereas T_{2D}^{-1} accounts for 78% of the total relaxation rate.

Let us next consider the ways in which the relaxation rates, T_{2B}^{-1}, T_{2S}^{-1} and T_{2D}^{-1}, of the small-grained natural magnetite mixtures, measured at t_E = 300μs (shown in Fig. 4), vary with magnetite concentration. We make the following observations: 1) T_{2B}^{-1} does not show a dependence on magnetite concentration and accounts for less than 1% of the total relaxation rate; 2) T_{2S}^{-1} increases with increasing magnetite concentration; 3) T_{2D}^{-1} decreases with increasing magnetite concentration. We find, as with the powdered synthetic magnetite mixtures, that the T_{2S}^{-1} values are consistently larger than the T_{2D}^{-1} and T_{2B}^{-1} values. At t_E = 300μs T_{2S}^{-1} accounts for over 90% of each of the total relaxation rates. At an echo time of 800μs, the contribution from the T_{2S}^{-1} values decreases but still accounts for over 50% of the total relaxation rate and the T_{2D}^{-1} values increase to account for the remainder of the total relaxation time.

Finally, let us next consider the ways in which the relaxation rates, T_{2B}^{-1}, T_{2S}^{-1} and T_{2D}^{-1}, of the large-grained natural magnetite mixtures, measured at t_E = 300μs (shown in Fig. 5), vary with magnetite concentration. 1) T_{2B}^{-1} shows no dependence on magnetite concentration within error of the measurement, and, in this case, T_{2B}^{-1} accounts for over 20%, of the total relaxation rate; 2) T_{2S}^{-1} increases with increasing magnetite concentration; 3) T_{2D}^{-1} shows a small increases with increasing magnetite concentration. As seen for the other mixtures, T_{2S}^{-1} values are larger than the T_{2D}^{-1} and T_{2B}^{-1} values, accounting for over 70% of the total relaxation rates. At an echo time of 800μs, the contribution from the T_{2S}^{-1} values does not decrease by much and still accounts for over 69% of the total relaxation rate. The T_{2D}^{-1} values only account for 0.5 to 2% of the total relaxation rate for t_E = 300 to 800μs.

To understand the effect of grain size on the relaxation rates we compare the values of T_{2B}^{-1}, T_{2S}^{-1}, and T_{2D}^{-1} for all the magnetite mixtures at a concentration of 1% for the natural magnetite mixtures and a concentration of 0.97% for the powdered synthetic magnetite mixtures we make the following observation: 1) T_{2B}^{-1} for all the mixtures is within 0.50 to 1.90s^{-1} and does not show a dependence on grain size; 2) T_{2S}^{-1} shows a dependence on grain size increasing from 2s^{-1} for the large-grained natural magnetite mixtures to 219s^{-1} for the powdered synthetic magnetite mixtures; and 3) T_{2D}^{-1} does not show a strong correlation with grain size. The T_{2D}^{-1} values of the small-grained natural magnetite and the powdered synthetic magnetite mixtures are the same within error but are two orders of magnitude larger than the T_{2D}^{-1} values for the large-grained natural magnetite.

The large differences in T_{2S}^{-1} for the samples of different grain sizes does not correspond to changes in the surface-area-to-volume ratios (Table 1) and so, as predicted in Eq. (6), must correspond to changes in ρ_2. The value of ρ_2 is proportional to the surface concentration of paramagnetic ions (C_p) (Foley

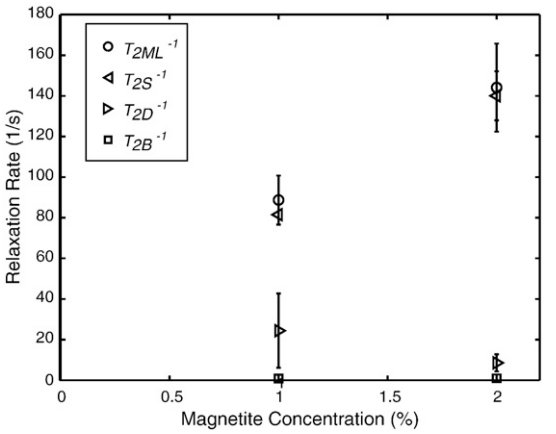

Fig. 4. Mean log average, surface, diffusion and bulk fluid relaxation rates versus magnetite concentration for water-saturated quartz sand mixed with small-grained natural magnetite. Errorbars not shown are smaller than the size of the data point.

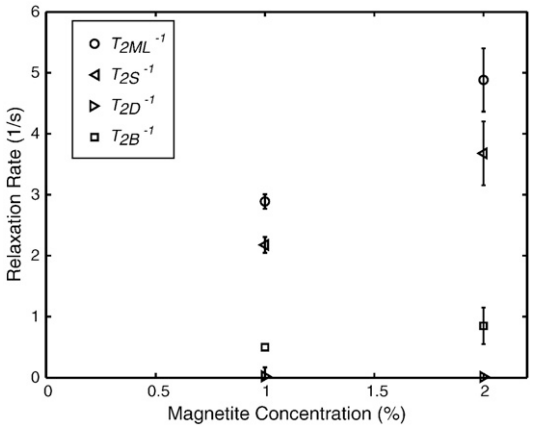

Fig. 5. Mean log average, surface, diffusion and bulk fluid relaxation rates versus magnetite concentration for water-saturated quartz mixed with large-grained natural magnetite. Errorbars not shown are smaller than the size of the data point.

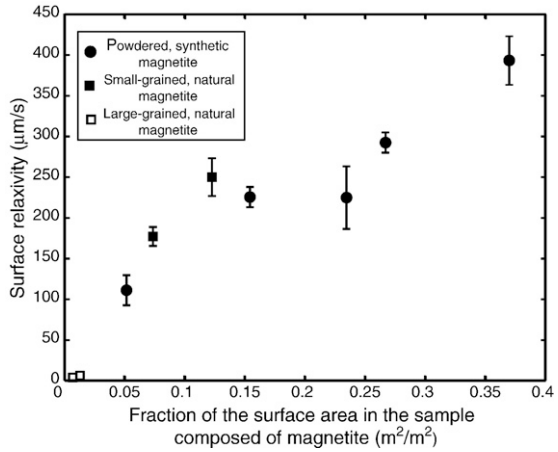

Fig. 6. Surface relaxivity versus the fraction of the surface area in the sample composed of magnetite for all the magnetite and quartz sand mixtures. Errorbars not shown are smaller than the size of the data point.

et al., 1996). This surface concentration can be represented as the fraction of the surface area containing paramagnetic ions. We can define C_p as:

$$C_p = \frac{S_p}{S_T} \tag{10}$$

where S_p is the surface area of the sample containing paramagnetic ions and S_T is the total surface area of the sample. In our study S_p can be assumed to be equivalent to the total surface area of magnetite present in the sample (S_M) resulting in the following definition for C_p:

$$C_p = \frac{S_M}{S_T} \tag{11}$$

The graph of ρ_2, calculated from Eq. (6), versus C_P (Fig. 6) shows that ρ_2 increases with an increase in the fraction of the surface area in the sample composed of magnetite.

The T_{2D}^{-1} values show no trend with increasing magnetic susceptibility, as would be expected due to the relationship between T_{2D}^{-1} and χ_m. We suspect that T_{2D}^{-1} is a function of the complex local magnetic field distribution within the pore space of a sample but leave it to another study to explore this relationship.

6. Conclusion

Using NMR relaxation rate measurements completed in this study we have determined the dominant relaxation mechanism for water-saturated sands in the presence of magnetite. We conclude that for all but one sample surface relaxation is the dominant relaxation mechanism. The exception is the powdered synthetic magnetite sample containing 1.4% magnetite; in this sample, at large echo times, the dominant relaxation mechanism is diffusion relaxation. Additionally, these results show that the surface relaxivity increases with an increase in total surface area of magnetite present in the sample per total surface area of the sample. Finally, these results did not find a strong correlation between diffusion relaxation rate and magnetite concentration or grain size.

While the data presented in this study have allowed us to recognize the link between the surface relaxivity and the fraction of the surface area in the sample composed of magnetite, further research is needed to understand, in more detail, the effect of magnetite on the surface and diffusion relaxation rates. One issue that needs to be addressed is the way in which the pore-scale distribution of the magnetite and its local effect on surface relaxivity affects the averaged surface relaxation rate and relaxivity calculated from the NMR relaxation time distributions. Another issue that remains to be addressed is the quantitative relationship between the local magnetic fields produced by the magnetite grains and the averaged diffusion relaxation rate calculated from the NMR relaxation time distributions.

Our research is focused on laboratory measurements designed to improve the understanding and interpretation of field measurements of NMR relaxation rates for environmental applications. We recognize that the precision of field measurements of NMR relaxation rates is currently limited due to technical issues associated with the available instruments. We are confident, however, that ongoing research to improve the field instrumentation will address these issues and lead to increased use of NMR as a valuable geophysical field method.

Acknowledgments

We would like to thank Christina Trotter for preparation of the natural magnetite samples, Gordon Brown for the use of his surface area analyzer, John Hillhouse for the use of the magnetic susceptibility analyzer, and the anonymous reviewers for their insightful comments. This work was supported in full by funding to Rosemary Knight under Grant DE-FG02-03ER15382-A0003 from the United States Department of Energy.

References

Berryman, J.G., 1995. Mixture theories for rock properties. In: Ahrens, T.J. (Ed.), Rock Physics and Phase Relations: A Handbook of Physical Constants. American Geophysical Union.

Bloembergen, N., Purcell, E.M., Pound, R.V., 1948. Relaxation effects in nuclear magnetic resonance absorption. Physical Review 73 (7), 679–715.

Brownstein, K.R., Tarr, C.E., 1979. Importance of classical diffusion in NMR studies of water in biological cells. Physical Review A 19 (6), 2446–2453.

Bryar, T.R., Knight, R.J., 2003. Laboratory studies of the effect of sorbed oil on proton nuclear magnetic resonance. Geophysical Research Letters 68 (3), 942–948.

Carr, H.Y., Purcell, E.M., 1954. Effects of diffusion on free precession in nuclear magnetic resonance experiments. Physical Review 94 (1), 630–638.

Clayton, N., 2006. Meeting oilfield developed geophysical logging in cased and uncased wells for high-resolution characterization of an alluvium ASR system in the Central Valley, California. Society of Exploration Geophysicists Hydrogeophysics Workshop. Vancouver.

Crook, N.P., Hoon, S.R., Taylor, K.G., Perry, C.T., 2002. Electron spin resonance as a high sensitivity technique for environmental magnetism: determination of contamination in carbonate sediments. Geophysical Journal International 149 (2), 328–337.

Dearing, J.A., 1999. Magnetic susceptibility. In: Walden, J., Oldfield, F., Smith, J. (Eds.), Environmental Magnetism: A Practical Guide. Technical Guide, 6. Quaternary Research Association, London, pp. 35–88.

Evans, M.E., Heller, F., 2003. Environmental Magnetism: Principles and Applications of Enviromagnetics. Elsevier Science.

Foley, I., Farooqui, S.A., Kleinberg, R.L., 1996. Effect of paramagnetic ions on NMR relaxation of fluids at solid surfaces. Journal of Magnetic Resonance 123, 95–104.

Godefroy, S., Korb, J.-P., Fleury, M., Bryant, R.G., 2001. Surface nuclear magnetic relaxation and dynamics of water and oil in macroporous media. Physical Review E 64, 21605–1–21605-13.

Hunt, C., Moskowitz, B.M., Banerjee, S.K., 1995. Magnetic properties of rocks and minerals. In: Ahrens, T.J. (Ed.), Rock Physics and Phase Relations: A Handbook of Physical Constants. American Geophysical Union.

Keating, K., Knight, R., 2007. A laboratory study to determine the effect of iron-oxides on proton NMR measurements. Geophysics 72 (1), E27–E32.

Korb, J.-P., Godefroy, S., Fleury, M., 2003. Surface nuclear magnetic relaxation and dynamics of water and oil in granular packings and rocks. Magnetic Resonance Imaging 21, 193–199.

Legchenko, A., Baltassat, J.-M., Beauce, A., Bernard, R., 2002. Nuclear magnetic resonance as a geophysical tool for hydrogeologists. Journal of Applied Geophysics 50, 21–46.

Meiboom, S., Gill, D., 1958. Modified spin-echo method for measuring nuclear relaxation times. Review of Scientific Instruments 29 (8), 688–691.

Oldfield, F., 1999. Environmental magnetism; the range of applications. In: Walden, J., Oldfield, F., Smith, J. (Eds.), Environmental Magnetism: A Practical Guide. Technical Guide, 6. Quaternary Research Association.

Seevers, D.O., 1966. A nuclear magnetic method for determining the permeability of sandstones. 7th SPWLA Transactions. Paper L.

Senturia, S.D., Robinson, J.D., 1970. Nuclear spin-lattice relaxation of liquids confined in porous solids. Society of Petroleum Engineers Journal 10, 237–244.

Shushakov, O.A., 1996. Groundwater NMR in conductive water. Geophysics 61 (4), 998–1006.

Smith, J., 1999. An introduction to the magnetic properties of natural materials. In: Walden, J., Oldfield, F., Smith, J. (Eds.), From: Environmental Magnetism: A Practical Guide. Technical Guide, 6. Quaternary Research Association.

Thompson, R., Oldfield, F., 1986. Environmental magnetism. Allen and Unwin.

Timur, A., 1969. Producible porosity and permeability of sandstones investigated through nuclear magnetic resonance principles. Log Analyst 10.

Trotter, C.E., 2001. Predicting the surface area to volume ratio of pores in iron rich sediments from nuclear magnetic resonance data. MSc Thesis. University of British Columbia.

Whittall, K.P., Bronskill, M.J., Henkelman, R.M., 1991. Investigation of analysis techniques for complicated NMR relaxation data. Journal of Magnetic Resonance 95, 221–234.